



**Comparison of
different evaporation
estimates**

P. Trambauer et al.

This discussion paper is/has been under review for the journal Hydrology and Earth System Sciences (HESS). Please refer to the corresponding final paper in HESS if available.

Comparison of different evaporation estimates over the African continent

**P. Trambauer¹, E. Dutra², S. Maskey¹, M. Werner^{1,3}, F. Pappenberger²,
L. P. H. van Beek⁴, and S. Uhlenbrook^{1,5}**

¹UNESCO-IHE, Department of Water Science and Engineering, P.O. Box 3015,
2601 DA Delft, the Netherlands

²ECMWF, Shinfield Park, RG2 9AX, Reading, UK

³Deltares, P.O. Box 177, 2600MH Delft, the Netherlands

⁴Utrecht University, Dept. Physical Geography, Utrecht, the Netherlands

⁵Delft University of Technology, Water Resources Section, P.O. Box 5048,
2600 GA Delft, the Netherlands

Received: 3 June 2013 – Accepted: 21 June 2013 – Published: 2 July 2013

Correspondence to: P. Trambauer (p.trambauer@unesco-ihe.org)

Published by Copernicus Publications on behalf of the European Geosciences Union.

Title Page	
Abstract	Introduction
Conclusions	References
Tables	Figures
◀	▶
◀	▶
Back	Close
Full Screen / Esc	
Printer-friendly Version	
Interactive Discussion	



Abstract

Evaporation is a key process in the water cycle, with implications ranging from water management, to weather forecast and climate change assessments. The estimation of continental evaporation fluxes is complex and typically relies on continental-scale hydrological or land-surface models. However, it appears that most global or continental-scale hydrological models underestimate evaporative fluxes in some regions of Africa, and as a result overestimate stream flow. Other studies suggest that land-surface models may overestimate evaporative fluxes. In this study, we computed actual evaporation for the African continent using a continental version of the global hydrological model PCR-GLOBWB, which is based on a water balance approach. Results are compared with other independently computed evaporation products: the evaporation results from the ECMWF reanalysis ERA-Interim and ERA-Land (both based on the energy balance approach), the MOD16 evaporation product, and the GLEAM product. Three other alternative versions of the PCR-GLOBWB hydrological model were also considered. This resulted in eight products of actual evaporation, which were compared in distinct regions of the African continent spanning different climatic regimes. Annual totals, spatial patterns and seasonality were studied and compared through visual inspection and statistical methods. The comparison shows that the representation of irrigation areas has an insignificant contribution to the actual evaporation at a continental scale with a 0.5° spatial resolution. The choice of meteorological forcing data has a larger effect on the evaporation results, especially in the case of the precipitation input as different precipitation input resulted in significantly different evaporation in some of the studied regions. ERA-Interim evaporation is generally the highest of the selected products followed by ERA-Land evaporation. The satellite based products (GLEAM and MOD16) do not show regular behaviour when compared to the other products, though this depends on the region and the season considered. The results from this study allow for a better understanding of the differences between products in each climatic region. Through an improved understanding of the causes of differences between these prod-

HESSD

10, 8421–8465, 2013

Comparison of different evaporation estimates

P. Trambauer et al.

Title Page

Abstract

Introduction

Conclusions

References

Tables

Figures



Back

Close

Full Screen / Esc

Printer-friendly Version

Interactive Discussion



ucts and their uncertainty, this study provides information to improve the quality of evaporation products for the African continent and, consequently, leads to improved water resources assessments at regional scale.

1 Introduction

5 Evaporation is one of the most important fluxes in the hydrological cycle. Recently, there has been a wide interest in estimating evaporation fluxes on a continental and global scales for a variety of purposes (van der Ent et al., 2010; Teuling et al., 2009; Miralles et al., 2011a; Vinukollu et al., 2011; Mu et al., 2011; Mueller et al., 2011, 2013; Jiménez et al., 2011). The accurate estimation of these fluxes on large scales
10 has, however, always been a difficult issue. Direct measurements of evaporation are only possible over small regions, e.g. using flux towers, and are limited to only few sites, particularly in some developed regions. Most of the existing global products are verified only in particular regions with available data, generally in North America and Europe (Mu et al., 2011; Alton et al., 2009; Zhang et al., 2010; Miralles et al., 2011b).
15 Some studies have evaluated the developed global evaporation product with evaporation estimates by subtracting runoff from the precipitation (Vinukollu et al., 2011; Zhang et al., 2010). Few studies have compared the results of different evaporation products. Vinukollu et al. (2011) compared results of six evaporation products (from three process based models forced with two radiation data sets) by computing the ensemble mean
20 and product range globally, and by comparing the annual totals of each product over latitude bands. The LandFlux initiative, supported by GEWEX (<http://www.gewex.org/>) is clearly dedicated to evapotranspiration. In the framework of this initiative, several global evaporation datasets were evaluated and compared (Jiménez et al., 2011; Mueller et al., 2011), and global merged benchmarking evaporation products were derived
25 (Mueller et al., 2013). To our knowledge, none of the existing studies regarding large scale evaporation has focused on the African continent. This work introduces a thor-

Comparison of different evaporation estimates

P. Trambauer et al.

Title Page

Abstract

Introduction

Conclusions

References

Tables

Figures

◀

▶

◀

▶

Back

Close

Full Screen / Esc

Printer-friendly Version

Interactive Discussion



ough comparison of different evaporation products over diverse African regions and climates.

In most cases, estimations of actual evaporation at a continental scale rely on complementary data such as (i) remote sensing, (ii) continental-scale hydrological models, or (iii) land surface models. However, in some ways, these three different data sources follow different theoretical basis or approaches in estimating evaporation. For example there is a significant difference in the model objective of land surface models and hydrological models. The former focus on providing boundary conditions (turbulent fluxes) to the atmosphere (mainly focusing on the energy balance) whereas the latter focus on closing the terrestrial water balance (Overgaard et al., 2006). In this study the class of hydrological models is represented by PCR-GLOBWB (van Beek and Bierkens, 2009). This model is based on the water balance approach that focuses on water availability and vertical and lateral transfer of water. The class of land-surface models is represented by the ECMWF reanalysis ERA-Land (Balsamo et al., 2012, ERA-L) and ERA-Interim (ERA-I, Dee et al., 2011) using a land surface model that describe the vertical exchanges of heat and water between the atmosphere and the land surface on a grid point scale (Balsamo et al., 2011a). The evaporation results of both are compared with the remote sensing based data (MOD16 product by Mu et al., 2011, 2007; and the GLEAM product by Miralles et al., 2011b). It is worth clarifying that PCR-GLOBWB and ERA-L evaporation come from offline (or stand alone) simulations, while ERA-I is a coupled land-atmosphere reanalysis product. The quality of the individual products can be influenced by different climatic regions. Therefore, in this study we differentiated the hydro-climatic regions in Africa and the comparison is carried out for each region.

The main aim of the present paper is to compare different actual evaporation estimates for the African continent in order to gain a better understanding of the disparities between the different products within defined regions and the possible causes of these differences (e.g. resulting from the meteorological input data or from the model structure in the derivation of actual evaporation). This understanding can lead to im-

HESSD

10, 8421–8465, 2013

Comparison of different evaporation estimates

P. Trambauer et al.

Title Page

Abstract

Introduction

Conclusions

References

Tables

Figures

⏪

⏩

◀

▶

Back

Close

Full Screen / Esc

Printer-friendly Version

Interactive Discussion



proved evaporation estimates for the African continent and, consequently, better water resources assessments.

2 Data and methods

2.1 Evaporation data sets

This section describes briefly the evaporation products used in this study (see Table 1 for a summary). These are all global products extracted for Africa at a daily temporal resolution, with the exception of MOD16 product, which is a monthly product. The period chosen in this study for the evaporation comparison is 2000–2010, which is the period common to all the products.

Four of the evaporation products considered in this study are based on the PCR-GLOBWB hydrological model (see Table 1, these products are indicated by the PCR prescript) with differences in the input data or addition of specific processes to assess their impact on the resulting evaporation product. Each of the products is described in detail below. The description of the first product based on PCR-GLOBWB also presents a general explanation of the PCR-GLOBWB hydrological model with the selected forcing data. We then describe the other PCR-GLOBWB based products by emphasizing only the differences to the first product.

2.1.1 PCR-GLOBWB

The PCR-GLOBWB evaporation product was calculated by means of a continental scale version of the distributed global hydrological model PCR-GLOBWB (van Beek and Bierkens, 2009), which was set up for the African continent. PCR-GLOBWB is a process based model that is applied on a cell-by-cell basis ($0.5^\circ \times 0.5^\circ$). PCR-GLOBWB is forced with potential evaporation, and actual evaporation is derived through simulation. Initially, the model converts potential reference evaporation E_0 into potential soil evaporation (ES_0) and potential transpiration (T_0) by introducing monthly and minimum

Comparison of different evaporation estimates

P. Trambauer et al.

Title Page

Abstract

Introduction

Conclusions

References

Tables

Figures

◀

▶

◀

▶

Back

Close

Full Screen / Esc

Printer-friendly Version

Interactive Discussion



Comparison of different evaporation estimates

P. Trambauer et al.

[Title Page](#)[Abstract](#)[Introduction](#)[Conclusions](#)[References](#)[Tables](#)[Figures](#)[◀](#)[▶](#)[◀](#)[▶](#)[Back](#)[Close](#)[Full Screen / Esc](#)[Printer-friendly Version](#)[Interactive Discussion](#)

crop factors. The crop factors are specified on a monthly basis for short and tall vegetation fractions, as well as for the open water fraction within each cell. These crop factors are calculated as a function of the Leaf Area Index (LAI) as well as of the crop factors for bare soil and under full cover conditions (van Beek et al., 2011). Interception evaporation reduces potential transpiration, and the availability of soil moisture storage is responsible for the reductions of the potential bare soil evaporation and transpiration. The potential bare soil evaporation over the unsaturated area is only limited by the unsaturated hydraulic conductivity of the upper soil layer. For the saturated area the rate of evaporation cannot exceed the saturated hydraulic conductivity of the upper soil layer. Transpiration only takes place for the unsaturated fraction of the cells and depends on the total available moisture in the soil layers (van Beek and Bierkens, 2009).

The model is described in full detail elsewhere (van Beek et al., 2011; van Beek and Bierkens, 2009). We hereby describe the forcing data applied in the first version of the model used in this study (product 1). Three other evaporation products were derived also from this model with changes in either the forcing data or in the model structure (products 2, 3 and 4, Table 1).

Meteorological forcing

The model is directly forced with daily precipitation, temperature and potential evaporation as calculated from other meteorological variables (2 m temperature, 2 m dew-point temperature, surface pressure, wind speed, and net radiation). Meteorological forcing was obtained from the ERA-Interim (ERA-Interim) reanalysis data of the past 32 yr (1979–2010). The ERA-Interim precipitation data used in this study is available at a resolution of approximately 0.7 degrees and was corrected with GPCP v2.1 (product of the Global Precipitation Climatology Project) to reduce the bias when compared to measured products (Balsamo et al., 2010; Szczypta et al., 2011). The GPCP v2.1 is available globally at $2.5^\circ \times 2.5^\circ$ resolution with a monthly frequency, covering the period from 1979 to September 2009. It combines the precipitation information available from

several sources (satellite data, rain gauge data, etc.) into a merged product (Szczypta et al., 2011; Huffman et al., 2009). The meteorological forcing was applied with the same spatial resolution of 0.5° as the model, using bilinear interpolation to downscale from the ERAI grid to the model grid, and is assumed to be constant over the grid cell.

5 Potential evaporation from reanalysis data

The PCR-GLOBWB model requires potential evaporation as a meteorological input, and this therefore needs to be estimated externally. There are several approaches to estimate potential evaporation, with diverse levels of data requirements and complexity, with different temporal scales, physically based and empirical, developed under specific regions or climates. The Hargreaves equation was used because it has the advantage to be applied in data scarce regions, which is the case for several regions in Africa. Droogers and Allen (2002) compared Penman-Monteith and Hargreaves reference evaporation estimates on a global scale and suggest that Hargreaves formula should be considered in regions where accurate weather data cannot be expected. The Hargreaves method requires less parameterization, leading to notably smaller sensitivity to error in climatic inputs (Hargreaves and Allen, 2003). Moreover, Sperna Weiland et al. (2012) studied several methods to calculate daily global reference potential evaporation from Climate Forecast System Reanalysis (CFRS) data from the National Center for Atmospheric Research, for application in a hydrological model study. They compared six different methods and found a re-calibrated form of the Hargreaves equation (increasing the multiplication factor of the equation from 0.0023 to 0.0031) to outperform the other alternatives.

2.1.2 PCR_PM

The PCR_PM evaporation product results from forcing the PCR-GLOBWB hydrological model with Penman-Monteith potential evaporation. The Penman-Monteith (P-M) method is one of the most widely used for the estimation of potential evaporation. Al-

Comparison of different evaporation estimates

P. Trambauer et al.

[Title Page](#)

[Abstract](#)

[Introduction](#)

[Conclusions](#)

[References](#)

[Tables](#)

[Figures](#)

[⏪](#)

[⏩](#)

[◀](#)

[▶](#)

[Back](#)

[Close](#)

[Full Screen / Esc](#)

[Printer-friendly Version](#)

[Interactive Discussion](#)



though this formula is in general highly recommended by the FAO and is considered to be one of the most physically based methods, it is impacted by the site aridity and is reported to underestimate the potential evaporation in some regions of Africa and other arid regions (Sperna Weiland et al., 2012; Hargreaves and Allen, 2003). Nevertheless, in this study we estimate the potential evaporation with the Penman-Monteith method using input variables derived from the ERAI data. This is then used to force the PCR-GLOBWB hydrological model to assess the difference in the actual evaporation resulting from the different inputs in potential evaporation. This product differs from the first product (PCR-GLOBWB) only in the forcing potential evaporation data set used.

2.1.3 PCR_TRMM

This evaporation product (PCR_TRMM) results from the PCR-GLOBWB hydrological model simulation, but forced with TRMM 3B42 v6 precipitation data, which has finer spatial resolution and is independent of the ERAI forecasting platform. Other meteorological inputs, including potential evaporation are as in the product 1 version of the PCR-GLOBWB model. Including this product in the comparison allows for assessing the impact that the precipitation forcing has on the resulting actual evaporation. The TRMM 3B42 v6 precipitation data was chosen from the available satellite-based rainfall estimates following the results of a recent study that validated six of these products and one reanalysis product (ERA-Interim) over four African basins (Thiemig et al., 2012), and found TRMM 3B42 together with RFE 2.0 (NOAA African Precipitation Estimation Algorithm) to be the most accurate products when compared to ground data.

2.1.4 PCR_Irrig

This product (PCR_Irrig) is also the result of the PCR-GLOBWB hydrological model when irrigation is included in the model structure. It was introduced in the study as some African countries such as Egypt, Morocco, Sudan and South Africa contain large irrigation areas. In South Africa, for example, there is a high density of small reser-

Comparison of different evaporation estimates

P. Trambauer et al.

[Title Page](#)

[Abstract](#)

[Introduction](#)

[Conclusions](#)

[References](#)

[Tables](#)

[Figures](#)

[◀](#)

[▶](#)

[◀](#)

[▶](#)

[Back](#)

[Close](#)

[Full Screen / Esc](#)

[Printer-friendly Version](#)

[Interactive Discussion](#)



HESSD

10, 8421–8465, 2013

Comparison of different evaporation estimates

P. Trambauer et al.

[Title Page](#)

[Abstract](#)

[Introduction](#)

[Conclusions](#)

[References](#)

[Tables](#)

[Figures](#)

[⏪](#)

[⏩](#)

[◀](#)

[▶](#)

[Back](#)

[Close](#)

[Full Screen / Esc](#)

[Printer-friendly Version](#)

[Interactive Discussion](#)



voirs for irrigation purposes (see McClain, 2012). The different components of evaporation (soil evaporation, transpiration and open water evaporation from reservoirs) are expected to increase as a result of irrigation practices, reaching potential evaporation rates under optimal irrigation practices. Moreover, a recent study by van Beek et al. (2011) suggested that the PCR-GLOBWB hydrological model might underestimate evaporation given that the model does not fully consider irrigated areas. They compared the PCR-GLOBWB evaporation results with the reanalyses ERA-40 (reanalysis by ECMWF, a previous version of the ERA-Interim) evaporation and found ERA-40 evaporation to be consistently higher than the evaporation data simulated by PCR-GLOBWB. They attributed these differences to irrigation, as they indicated that ERA-40 (which includes data assimilation) accounts implicitly for irrigation by decreasing the temperature to compensate for the energy loss as latent heat. The original version of PCR-GLOBWB, on the other hand, includes irrigated areas using crop factors, but actual evaporation cannot exceed the available soil moisture as the additional contribution due to irrigation is not modelled. The difference between the two actual evaporation products represent the transpiration of the water applied (van Beek et al., 2011).

To include the influence of irrigation the original PCR-GLOBWB hydrological model was adapted. The irrigation requirement for the irrigated crop area within a cell is supplied through the storage of freshwater in the cell. For each cell where irrigation takes place, it is assumed that at least a small farm reservoir is included and that this provides sufficient storage to satisfy the demand. The irrigated area within each cell, water requirements and irrigation cropping patterns are extracted from the “Global map of irrigated areas” from Siebert et al. (2007) and FAO (1997). This modified version of the hydrological model serves to assess the impact of adding irrigation in the model structure on the actual evaporation results.

2.1.5 ERAI

ERA-Interim (ERAI) is a global atmospheric reanalysis produced by the European Centre for Medium-Range Weather Forecasts (ECMWF) which covers the period from Jan-

uary 1979 to present date with a horizontal resolution of approximately 0.7 degrees and 62 vertical levels. A comprehensive description of the ERAI product is available in Dee et al. (2011). The ERAI evaporation is the result from the coupled land-atmosphere simulations. The ERAI land component is the model TESSEL (Van den Hurk et al., 2000) that is coupled to the atmospheric model, therefore being forced (and providing fluxes to the atmosphere) with the ERAI forecasts of near surface conditions (temperature, humidity, pressure and wind speed) and downward energy and water fluxes (precipitation, solar and thermal radiation).

2.1.6 ERAL

ERA-Land (ERAL, Balsamo et al., 2012) is a global land-surface data set covering the period 1979–2010. ERA-Land is a land-surface only simulation (offline) carried out with HTESSEL (Balsamo et al., 2011a, b), an updated version of TESSEL (that was used in ERAI), with meteorological forcing from ERAI and precipitation adjustments based on GPCP. HTESSEL computes the land surface response to the near surface atmospheric conditions forcing, and estimates the surface water and energy fluxes and the temporal evolution of soil temperature, moisture content and snowpack conditions. At the interface to the atmosphere each grid box is divided into fractions (tiles), with up to six fractions over land (bare ground, low and high vegetation, intercepted water, shaded and exposed snow). The grid box surface fluxes are calculated separately for each tile, leading to a separate solution of the surface energy balance equation and the skin temperature. The latter represents the interface between the soil and the atmosphere. Below the surface, the vertical transfer of water and energy is performed using four vertical layers to represent soil temperature and moisture. Soil heat transfer follows a Fourier law of diffusion, modified to take into account soil water freezing/melting. Water movement in the soil is determined by Darcy's Law, and surface runoff accounts for the sub-grid variability of orography (Balsamo et al., 2009). HTESSEL is part of the integrated forecast system at ECMWF with operational applications ranging from short-range to monthly and seasonal weather forecasts.

Comparison of different evaporation estimates

P. Trambauer et al.

[Title Page](#)

[Abstract](#)

[Introduction](#)

[Conclusions](#)

[References](#)

[Tables](#)

[Figures](#)

[◀](#)

[▶](#)

[◀](#)

[▶](#)

[Back](#)

[Close](#)

[Full Screen / Esc](#)

[Printer-friendly Version](#)

[Interactive Discussion](#)



2.1.7 MOD16

Remote sensing provides an indirect method to estimate global actual and potential evaporation. MOD16 is described in detail by Mu et al. (2011, 2007), and computes potential and actual evaporation using MODIS (Moderate resolution Imaging Spectroradiometer) land cover, albedo, leaf area index (LAI), an Enhanced Vegetation Index (EVI), and a daily meteorological reanalysis data set from NASA's Global Modelling and Assimilation Office (GMAO) as inputs for regional and global evaporation mapping and monitoring (Mu et al., 2011). This method is an adaptation of a previous version of the evaporation algorithm by Mu et al. (2007), which is based on the remotely sensed evaporation model developed by Cleugh et al. (2007).

Mu et al. (2011) computed potential evaporation with the Penman-Monteith method driven by GEOS-5 daily meteorological reanalysis inputs and MODIS derived vegetation data: land surface temperature, leaf area index (LAI), gross primary productivity and vegetation indices were extracted from four different MODIS products. To derive actual from potential evaporation Mu et al. (2007) include multipliers to halt plant transpiration and soil evaporation as follows: low temperatures and water stress (due to high vapour pressure deficit) limit the transpiration flow, and soil evaporation is limited by a complementary relationship hypothesis which defines land-atmospheric interactions from vapour pressure deficit and relative humidity (Mu et al., 2007).

This product has been validated against actual measurements in several regions. Mu et al. (2011) evaluated their algorithm using evaporation observations at 46 eddy covariance flux towers in the United States and Canada. In their paper they present the Root Mean Square Error (RMSE), correlation, and Taylor skill score for each flux tower, and they report that the average mean absolute bias values are 24.1 % of the evaporation measurements. Kim et al. (2012) validated MOD16 global terrestrial evaporation products at 17 flux tower locations in Asia and found good agreement only at five locations ($r = 0.50$ to 0.76 , bias = -1.42 to $1.99 \text{ mm } 8\text{d}^{-1}$; RMSE = 1.99 to $8.96 \text{ mm } 8\text{d}^{-1}$). They observed the best performance of the MOD16 evaporation algorithm at sites with

HESSD

10, 8421–8465, 2013

Comparison of different evaporation estimates

P. Trambauer et al.

Title Page

Abstract

Introduction

Conclusions

References

Tables

Figures

◀

▶

◀

▶

Back

Close

Full Screen / Esc

Printer-friendly Version

Interactive Discussion



forested land cover. They observed poor performance at sites with grassland cover in arid and polar climates. The MODIS derived potential and actual evaporation are available online (<http://www.ntsug.umd.edu/project/mod16>) with a resolution of 1 km and as with most standard MODIS Land products, it uses the Sinusoidal grid tiling system in which the tiles are 10 degrees by 10 degrees at the equator (USGS, 2012) We created the mosaic for each month obtaining one monthly map for the entire continent, and we upscaled them to a resolution of 0.5 degrees (~ 50 km) using the cubic convolution resampling as suggested by Keys (1981) and Liu et al. (2007).

2.1.8 GLEAM

GLEAM (Global Land surface Evaporation: the Amsterdam Methodology) is a recent global evaporation product with a 0.25 degree spatial resolution developed in the VU University of Amsterdam (Miralles et al., 2011b) mainly based on satellite observations. This version of the model is forced with PERSIANN (Precipitation Estimation from Remotely Sensed Information using Artificial Neural Networks) precipitation data, soil moisture and vegetation optical depth from the NASA-LPRM (Land Parameter Retrieval Model, Owe et al., 2008), radiation fluxes from ERA-Interim, air temperature from AIRS (Atmospheric InfraRed Sounder) gap-filled with ISCCP (International Satellite Cloud Climatology Project, Rossow and Schiffer, 1999), and snow water equivalents from NSIDC (National Snow and Ice Data Center, Armstrong et al., 2007). The GLEAM methodology uses the Priestley and Taylor (PT) evaporation model and several satellite-sensor products to estimate global daily evaporation. The GLEAM algorithm was validated against one year of eddy covariance measurements from 43 stations in North America, showing a good model performance in all vegetation types and climate conditions (average correlation coefficient of $R = 0.83$ for daily time series, and $R = 0.90$ for monthly time series) (Miralles et al., 2011b).

HESSD

10, 8421–8465, 2013

Comparison of different evaporation estimates

P. Trambauer et al.

Title Page

Abstract

Introduction

Conclusions

References

Tables

Figures

◀

▶

◀

▶

Back

Close

Full Screen / Esc

Printer-friendly Version

Interactive Discussion



2.2 Definition of regions

In this paper we aim to compare the different sets of evaporation results in defined African regions. With this purpose, we divided the African continent in regions based on similar aridity conditions and annual precipitation cycles. First, we divided the African continent based on climatic classes. The classification of the different climates was done following the definition of the UNEP (1997) and the Global Aridity Index (Global-Aridity) data set produced by Zomer et al. (2008). This is published online in the Consultative Group for International Agriculture Research Consortium for Spatial Information (CGIAR-CSI) website (CGIAR CSI Consortium for Spatial Information, 2010). The Global-Aridity data set is provided for non-commercial use in standard ARC/INFO Grid format, at 30 arc seconds (~ 1 km at equator). Zomer et al. (2008) calculated a global map of the mean Aridity Index (AI) from the 1950–2000 period at 30' spatial resolution (equivalent to half-degree) as:

$$AI = MAP/MAE \quad (1)$$

where MAP is the Mean Annual Precipitation (mm yr^{-1}) and MAE is the Mean Annual Potential Evaporation (mm yr^{-1}) (Zomer et al., 2008). In their study, Zomer et al. (2008) computed the mean Aridity Index using the data available from the WorldClim Global Climate Data (Hijmans et al., 2005) as input parameters and the Hargreaves equation to model Potential Evaporation globally.

For the purpose of this study, we processed this AI global data set in GIS, trimmed it for the African continent, classified it into six classes according to the UNEP classification (1997) (see Table 2), and upscaled it to a grid resolution of 0.5 degrees in agreement with the hydrological model grid. For upscaling we used the area-majority technique. Figure 1 presents the resulting map of climate classes for the African continent at the upscaled resolution.

Different regions of the continent have very diverse annual precipitation cycles despite being classified in the same climate class. This is the case, for example, of the

HESSD

10, 8421–8465, 2013

Comparison of different evaporation estimates

P. Trambauer et al.

Title Page

Abstract

Introduction

Conclusions

References

Tables

Figures

◀

▶

◀

▶

Back

Close

Full Screen / Esc

Printer-friendly Version

Interactive Discussion



Comparison of different evaporation estimates

P. Trambauer et al.

Title Page

Abstract

Introduction

Conclusions

References

Tables

Figures

⏪

⏩

◀

▶

Back

Close

Full Screen / Esc

Printer-friendly Version

Interactive Discussion



arid climate in the Horn of Africa and in South-Western Africa, one characterized by two rainy seasons and another by only one rainy season in a year (see McClain, 2012). This is why most studies that divide Africa in regions usually consider sub-regions that capture the mean annual cycle of precipitation of the region (single or multiple rainy seasons, precipitation interannual variability, etc.). Sylla et al. (2010) divided the continent in eight regions, namely: West Sahel, East Sahel, Guinea Coast, North equatorial central Africa, Horn of Africa, South equatorial central Africa, Central Southern Africa, and South Africa. These regions have a uniform annual cycle of precipitation but do not distinguish between the different climatic classes within the region. The total annual precipitation in the Sahel region can be much higher for the semi-arid climate than for the arid climate (both contained in the Sahel region).

This study differentiates in regions characterized by both the regional location (e.g. Horn of Africa or Southern Africa) and the climatic class within the region. We merged some of the regions defined by Sylla et al. (2010) which had very similar mean annual cycles of precipitation (e.g. East Sahel with West Sahel, Central Southern Africa with South Africa), to reduce the number of sub-regions from eight to five. To these we added the Mediterranean Region. Six location-regions were therefore defined and are presented in Fig. 2. Finally each location-region was divided in their climatic class and the resulting regions are shown in Fig. 3. The Sahara desert region was not considered in this study due to the negligible evaporation rates year round by virtue of hyper-arid conditions that result in very low water content in the soil.

2.3 Comparison of evaporation products

The common period January 2000 to December 2010 was selected to compare the evaporation products for this study. We first evaluate the difference between the crop-specific potential evaporation products that are used in this study for the derivation of the actual evaporation products (if applicable). The crop-specific potential evaporation, PET_c (mm day^{-1}) is computed within the PCR-GLOBWB model from: $PET_c = k_c \times PET_r$, where PET_r (mm day^{-1}) is the reference potential evaporation and k_c is a crop factor

(dimensionless) (van Beek et al., 2011). The comparison between the actual evaporation products is then carried out at a monthly temporal scale as well as within the defined regions in the continent.

Continental maps of long-term average annual potential evaporation were computed for each product. To compare two of the evaporation products on a gridded basis, and considering the absence of ground data to compare to, we defined the relative mean difference (RMD (%)) of the two evaporation products as:

$$\text{RMD} = \frac{(E_1 - E_2)}{\bar{E}} \times 100\% \quad (2)$$

where E_1 and E_2 is the annual evaporation (mm yr^{-1}) data set of 1 or 2, respectively, and \bar{E} is the mean evaporation (mm yr^{-1}) of products E_1 and E_2 .

RMD indicates which product is consistently higher than the other, and the relative magnitude of the difference between them (compared with the average value). This indicator seems to be a fair way of estimating the relative difference as none of the available products represents ground truth. Indicators showing absolute differences are not useful as the same absolute difference can be relatively large for areas with low actual evaporation values (arid areas), and relatively low for areas with high actual evaporation values (humid areas).

We also computed continental maps of long-term average actual evaporation for each product to allow for a visual perception of the spatial variability of the continental evaporation for each product, and between products. Moreover, to make the analysis quantitative, we created an Evapotranspiration Multiproduct (EM) as the median of the considered products and we computed the Relative Mean Bias (RMB (%)) between each product and the EM. In this case we considered the EM as the “observations”, and the RMB was defined similarly to the RMD as follows:

$$\text{RMB} = \frac{(E_i - \text{EM})}{\text{EM}} \times 100\% \quad (3)$$

HESSD

10, 8421–8465, 2013

Comparison of different evaporation estimates

P. Trambauer et al.

Title Page

Abstract

Introduction

Conclusions

References

Tables

Figures

◀

▶

◀

▶

Back

Close

Full Screen / Esc

Printer-friendly Version

Interactive Discussion



where E_i is the annual actual evaporation (mm yr^{-1}) data set i and EM is the annual actual evapotranspiration multiproduct (mm yr^{-1}).

Subsequently, for each region the annual totals of each evaporation product were computed and the seasonality of the different products was studied and compared with the EM. The mean annual anomalies of each product with respect to the EM are presented for each region, and the inter-annual variation of mean monthly actual evaporation was plotted for each product within each region and compared through visual inspection. The statistics of each evaporation product were then plotted for each region by means of Taylor diagrams of monthly evaporation and a box-plot diagram of seasonal evaporation. The box-plots are displayed for the wet and the dry seasons.

3 Results

3.1 Comparison of potential evaporation products

Figure 4 presents the mean annual crop-specific potential evaporation for the period 2000–2010 based on (a) the Penman-Monteith method, and (b) the Hargreaves method, both derived from the ERA-Interim reanalysis data. Figure 4c presents the potential evaporation from the MOD16 product, which uses the Penman-Monteith method but is derived from NASA's Global Modelling and Assimilation Office (GMAO) meteorological data and MODIS maps. The areas in grey in the MOD16 potential evaporation correspond to missing evaporation data in the MOD16 product. These are mainly in the hyper-arid and arid areas with sparsely vegetated or with barren soils. The other products included in this study do not compute or provide the potential evaporation.

As can be seen in Fig. 4a and b, the potential evaporation derived from the Penman-Monteith equation and Hargreaves equation result in very similar values throughout the continent. The potential evaporation from MOD16, on the other hand, results in much higher values than the ones derived from the other two methods, especially for arid and semi-arid areas. The differences are such (a factor of 2 or up to 3) that the map needs to

Comparison of different evaporation estimates

P. Trambauer et al.

Title Page

Abstract

Introduction

Conclusions

References

Tables

Figures

◀

▶

◀

▶

Back

Close

Full Screen / Esc

Printer-friendly Version

Interactive Discussion



be presented with a different scale. The high disparities between the different potential evaporation products seem to be quite common, as also reported in Sperna Weiland et al. (2012), Weiß and Menzel (2008) and Kingston et al. (2009). Figure 5 presents the Relative Mean Difference (RMD) between each pair of products, and shows that the difference between the MOD16 potential evaporation product with the other two products is much smaller in humid areas than in arid and semi-arid areas. Penman-Monteith and Hargreaves products present RMD smaller than 20 % throughout the continent.

3.2 Comparison of actual evaporation products

3.2.1 Mean annual evaporation

From the maps of mean annual evaporation for each product (not shown) it appears that the similarity between the different actual evaporation products is much higher than it is between the potential evaporation products. This suggests that the high variability introduced by the potential evaporation products is decreased in the derivation of actual evaporation. Figure 6 shows the maps of RMB between the mean annual actual evaporation of each product and the EM for the period 2000–2010. The RMB results in the highest values for the hyper-arid areas in the Sahara desert, region that was left out of this analysis due to its negligible actual evaporation values. It can also be observed that mean annual evaporation maps of the PCR-GLOBWB and the PCR_Irrig products are almost identical (with the exception of some few regions). For this reason, PCR_Irrig product was not considered in the EM product to avoid a double weight. ERAI is generally considerable above the EM, and for the remaining products the offset with the EM depends on the region. Over some water bodies higher evaporation values are noticeable in the products resulting from the PCR-GLOBWB model when compared to the other products, as open water evaporation is considered in the total actual evaporation in this model.

Comparison of different evaporation estimates

P. Trambauer et al.

[Title Page](#)

[Abstract](#)

[Introduction](#)

[Conclusions](#)

[References](#)

[Tables](#)

[Figures](#)

[⏪](#)

[⏩](#)

[◀](#)

[▶](#)

[Back](#)

[Close](#)

[Full Screen / Esc](#)

[Printer-friendly Version](#)

[Interactive Discussion](#)



The annual anomalies of evaporation for each product with respect to the EM are presented in Fig. 7 for each region. The figure shows that ERAI evaporation product has the highest annual evaporation in the continent for almost every region with the exception of the hyper-arid and arid areas of the Mediterranean (R2 and R3) and Sahel (R4 and R5) regions, which border the Sahara desert. Regarding the other evaporation products, in most cases they deviate from the EM for less than 100 mm yr^{-1} , with some few exceptions for MOD16, PCR_TRMM and GLEAM. The PCR-GLOBWB derived products forced with ERAI + GPCP precipitation are in almost every case close to the EM with the exception of humid Sahel (R8). PCR_TRMM product (PCR-GLOBWB model forced with TRMM precipitation data) is mostly lower than the EM (with the exception of the regions bordering the Sahara desert), and closer to GLEAM, both forced with satellite rainfall products.

3.2.2 Monthly and seasonal evaporation

Figure 8 shows how the different evaporation products follow the inter-annual variability. For each region the mean monthly actual evaporation for every product and the EM is plotted. Seasonality is highlighted in the figure. We defined the seasons in the continent as dry and wet, and the wet seasons for each region are indicated with a grey shadow in Fig. 8. The statistics of the seasonal evaporation during the wet and dry seasons are presented graphically in Fig. 9 by means of a box-plot diagram, showing the variability of the seasonal evaporation for each product within each region. Additionally, the statistics of monthly evaporation are presented in Taylor diagrams for each region (see Fig. 10), which summarize the ratio of the standard deviation of each product and the EM, their root-mean-square difference (RMSD, showed in grey curves in Fig. 10), and the temporal correlation between each product and EM (based on the monthly values 2000–2010). The EM is considered here as the “reference” field. In the Taylor diagrams, products that are closer to the reference field have a “higher performance” than those which are farther, which in this study is interpreted as higher consistency between the products.

Comparison of different evaporation estimates

P. Trambauer et al.

Title Page

Abstract

Introduction

Conclusions

References

Tables

Figures

◀

▶

◀

▶

Back

Close

Full Screen / Esc

Printer-friendly Version

Interactive Discussion



Large scale analysis

In general terms, introducing the irrigation process in such a large scale-analysis does not result in visible changes. This can be observed in Figs. 7, 8, 9 and 10, where only in the Mediterranean region (R1, R2 and R3) and in the semi-arid Horn of Africa (R14) a slight deviation between the evaporation products with and without irrigation can be observed. In the regions where the larger irrigation areas in the continent are located (e.g. Nile Delta), the evaporation estimate when irrigation is considered is slightly higher than when irrigation is not considered. Introducing irrigation therefore does not significantly bring the evaporation closer to the ERA-Interim product at this scale, as the higher evaporations in the comparatively small irrigated areas become insignificant when merging these values over larger areas without irrigation. In Figs. 8 and 10 PCR_Irrig product is in general overlapping with the PCR-GLOBWB product.

Another feature that is clearly visible from Figs. 7, 8 and 9 is that for almost every region and season ERAI product consistently has the highest evaporation. ERAI evaporation is in almost every case lower than that of ERAI. ERAI and ERAL differ mainly in three aspects: (i) land surface model: TESSEL in ERAI and HTESSEL in ERAL; (ii) coupling to the atmosphere: ERAI coupled and ERAL land surface only simulations (no feedback to the atmosphere forced with corrected precipitation); and (iii) data assimilation: none in ERAL while ERAI soil moisture assimilation scheme corrects soil moisture in the first three layers based on the 6 h atmospheric analysis increments of specific humidity and temperature at the lowest model level (Douville et al., 2000). While the first two points are difficult to evaluate, the impact of soil moisture data assimilation in ERAI can be evaluated by calculating the assimilation increments: i.e. the amount of soil moisture added (or removed) by the data assimilation system. Figure 11 shows the mean annual soil moisture increments in ERAI. The increments are positive in most of the African continent, and partly explain the higher values of evaporation in ERAI when compared with ERAL. The results in this study do not allow to clearly identify the main

HESSD

10, 8421–8465, 2013

Comparison of different evaporation estimates

P. Trambauer et al.

Title Page

Abstract

Introduction

Conclusions

References

Tables

Figures

◀

▶

◀

▶

Back

Close

Full Screen / Esc

Printer-friendly Version

Interactive Discussion



source of the differences between ERAI and ERAL, but qualitatively, ERAL is closer to the remaining data sets.

Regarding the impact that input meteorological data has on the resulting evaporation we should look at both input precipitation and input potential evaporation. With respect to the input precipitation, there seems to be a general behaviour showing that the evaporation resulting from the model forced with TRMM precipitation is consistently lower than the evaporation that results when the model is forced with ERAI + GPCP (see Figs. 7, 8 and 9). For almost every region, TRMM forced model results in lower evaporations than the EM. Regarding the potential evaporation input, it can be seen that the evaporation generated with Penman-Monteith potential evaporation is in every case very similar to the one forced with Hargreaves.

The MOD16 evaporation show poor consistency with the other products in arid areas (Kim et al., 2012, observed poor performance of this product for arid areas); this can be seen in Figs. 8 and 10 for regions R2 to R5 and R21 where in some cases the product representation it is even out of the Taylor plot. For other regions, mainly in the dry-sub humid and semi arid climatic regions, MOD16 is more consistent with the other products (see Fig. 10 for R7, R8 and R17 to R20).

Regional analysis

Mediterranean region (R1 to R3)

This region is characterized by higher evaporation rates in the months of March to May, after the end of the rainy season (see Fig. 8). The evaporation peak is clear in the Semi-Arid region (R1), but becomes less noticeable in the arid region (R2) as the evaporation rates become lower and almost disappear in the hyper-arid areas (R3) where evaporation rates throughout the year are negligible. In the rainy season Figs. 8 and 9 show a clear offset between ERAI and ERAL with respect to the other products, where the first two present considerably higher evaporation rates. In the dry season, while ERAL comes closer to the other products, the offset of ERAI is still evident.

Comparison of different evaporation estimates

P. Trambauer et al.

Title Page

Abstract

Introduction

Conclusions

References

Tables

Figures

◀

▶

◀

▶

Back

Close

Full Screen / Esc

Printer-friendly Version

Interactive Discussion



This offset of ERAI in the dry periods decreases with increasing aridity, in contrast with the MOD16 product, which shows higher evaporation rates than the remaining datasets for arid areas (R2) in the dry period. In the Mediterranean region only the dry season of the semi-arid region (R1) presents quite a high variability between the different seasons for every product (Fig. 9). Figure 10 shows that for the semi-arid Mediterranean region (R1) most products are quite similar to the EM with the exception of ERAI and MOD16 which are poorly correlated. As aridity increases, the consistency between the products deteriorate and in hyper-arid Mediterranean region (R3) all the products show very little consistency.

Sahel (R4 to R8)

The Sahel region is characterized by an annual evaporation cycle with one peak during the rainy season, namely from July to September (Sylla et al., 2010) (see Fig. 8). The evaporation rates become higher and the peaks become clearer with increasing humidity. Figure 8 shows that only the MOD16 product in the arid region (R5) and to a less extent in the semi-arid region (R6) do not capture the annual evaporation cycle, presenting a relatively uniform evaporation throughout the year. This can also be seen in Fig. 10 where the very low values of normalized standard deviation in MOD16 indicate that the amplitude of the annual cycle is underestimated. Figures 8 and 9 show that the lowest evaporation values are observed for PCR_TRMM during the dry season but it is not clear for the wet season. Regarding the highest evaporation values, ERAI (and secondly ERAI) present these during the dry season, but a clear behaviour cannot be observed for the wet season. The semi-arid (R6), dry-sub-humid (R7) and humid Sahel (R8) are the regions that present the largest variability in the inter-annual mean cycles for each product and the higher dispersion between the products in the dry seasons. Similarly to the Mediterranean region, the hyper-arid region (R4) in the Sahel shows the least consistency between all the products (see Fig. 10). Figure 10 shows that for the other sub-regions all the products

HESSD

10, 8421–8465, 2013

Comparison of different evaporation estimates

P. Trambauer et al.

[Title Page](#)

[Abstract](#)

[Introduction](#)

[Conclusions](#)

[References](#)

[Tables](#)

[Figures](#)



[Back](#)

[Close](#)

[Full Screen / Esc](#)

[Printer-friendly Version](#)

[Interactive Discussion](#)



have a higher consistency with the exception of MOD16 for R5 and R6 that was already discussed, and ERAI and PCR_TRMM for R8. The figure shows that in the Sahel region ERAI product slightly underestimate the annual cycle amplitude when compared to the EM, and PCR-PM, and PCR_TRMM slightly overestimate of this amplitude, while all the products are correctly phased (high correlation).

Guinean coast and north equatorial central Africa (R9 to R12)

This region is characterized by a bimodal precipitation cycle with unpronounced peaks and precipitation minima. This precipitation pattern results in different evaporation cycles depending on the aridity of the region (see Fig. 8). For the humid region (R9) all products show more or less uniform evaporation over the year; however, respective values between the products are different (see Fig. 10). In regions R10 and R11 the majority of the products follow roughly the same pattern, with slightly noticeable peaks around May and October. MOD16 deviates from this pattern, represents the amplitude fairly well in the annual cycle but remains out of phase (see Fig. 10). Figure 8 shows that the peaks of the evaporation cycle become more pronounced when aridity increases. The arid area (R12) has a clear bimodal evaporation cycle. For this region (R12) the GLEAM product presents the lowest values throughout the year. During the dry season ERAI present the highest values; while during the wet season a clear behaviour cannot be observed. Figure 10 suggests that most of the products have a good consistency in R10 and R11 with the exception of MOD16, while in R12 the products show less consistency.

Horn of Africa (R13 and R14)

The Horn of Africa presents a bimodal evaporation cycle with defined peaks at around May and November (see Fig. 8). For this region most products show little consistency. This can be observed both in Figs. 8 and 10. In the arid Horn of Africa

HESSD

10, 8421–8465, 2013

Comparison of different evaporation estimates

P. Trambauer et al.

Title Page

Abstract

Introduction

Conclusions

References

Tables

Figures

⏪

⏩

◀

▶

Back

Close

Full Screen / Esc

Printer-friendly Version

Interactive Discussion



Comparison of different evaporation estimates

P. Trambauer et al.

Title Page

Abstract

Introduction

Conclusions

References

Tables

Figures

◀

▶

◀

▶

Back

Close

Full Screen / Esc

Printer-friendly Version

Interactive Discussion



(R13) ERAI and ERAI present larger amplitude of the annual cycle than the EM, and MOD16 shows lower amplitude of the annual cycle than the EM. In the semi-arid region (R14) the amplitude of the annual cycle are now consistent between most products (normalized standard deviation close to one), but the correlation coefficients are rather low (the time series are not correctly phased).

Southern equatorial central Africa (R15 to R17)

This region presents an evaporation seasonal cycle with a minimum in June through October and a maximum in December through April (see Fig. 8). The difference between the evaporation values in the wet and in the dry season increases with aridity. The consistency between all products seems to be quite better in the dry-sub-humid region (R16) than in the humid region (R15). In R15 MOD16 and ERAI seem to be fairly out of phase (low correlation values), and PCR_TRMM presents a larger amplitude of the annual cycle than the EM. Regarding the semi-arid region (R17), the absolute amplitude of the annual cycle increases, and quite a good consistency is observed between all the products.

Southern Africa (R18 to R21)

The Southern Africa region show a pronounced seasonal cycle with a minimum in June through October and a maximum in December through April (see Fig. 8). In the semi-arid (R18), humid (R19) and dry-sub-humid (R20) regions all the products present a good consistency (see Fig. 10). In the semi-arid (R18) and arid (R21) regions MOD16 presents a lower annual cycle amplitude that the EM, which is represented in Fig. 10 by low normalized standard deviations. In the arid region (R21) all the products show less consistency.

to higher surface runoff, which also keeps the water out of reach of evaporation and results in lower evaporation. For the scale considered in this study, it is clear that rainfall events with higher intensities result in lower evaporation values (see Figs. 7 and 8) as a result of higher surface runoff, given that PCR_TRMM evaporation is generally lower than PCR-GLOBWB evaporation.

The difference between the evaporation products PCR_TRMM and PCR-GLOBWB is not negligible and it varies from region to region, and therefore is important to force the hydrological model with the most suitable precipitation product for that particular region. Thiemig et al. (2012) found TRMM together with RFE to be the best satellite products available for the African continent. However, they noted that both TRMM and ERAI underestimate the amount of rainfall during the heavy rainfall events, and they explained that for the satellite products this was mainly the result of the small extent of the heavy precipitation cells, which are generally lower than the detection limit of the satellite sensors. While ERAI highly overestimates the number of rainy days, TRMM also has some overestimation of the rainy days for tropical wet and dry zones but lower than that of ERAI (Thiemig et al., 2012). Moreover, Wang et al. (2009) highlights some known “anomalies” in TRMM such as underestimation in “warm-rain” regimes. In these regimes rain is derived from non icephase processes in clouds (see Lau and Wu, 2003, for detailed explanation).

4.1.2 Potential evaporation data

The potential evaporation used as a forcing appears to have some influence in the estimation of actual evaporation in some of the regions. The PCR-GLOBWB hydrological model was forced with two sets of reference potential evaporation products to assess the weight that this input has on the results. The resulting evaporation product PCR_PM (model forced with Penman-Monteith potential evaporation) is in general slightly higher than the PCR product (hydrological model forced with Hargreaves potential evaporation) and more similar to the EM. The forcing potential evaporation seems to have less influence on the actual evaporation results than the forcing precipitation, but this might

HESSD

10, 8421–8465, 2013

Comparison of different evaporation estimates

P. Trambauer et al.

Title Page

Abstract

Introduction

Conclusions

References

Tables

Figures

◀

▶

◀

▶

Back

Close

Full Screen / Esc

Printer-friendly Version

Interactive Discussion



be due to the fact that the original difference between the two potential evaporation products was quite small.

4.2 Effect of the model structure in the estimation of actual evaporation

The comparison between the PCR-GLOBWB and the PCR_Irrig evaporation products can help us identify the effect of introducing an irrigation scheme in a hydrological model on simulated actual evaporation. The only difference between these two models is the introduction of the irrigation scheme in PCR_Irrig which was not included in PCR-GLOBWB. A recent study by van Beek et al. (2011) attributed partly the difference between PCR-GLOBWB simulated actual evaporation and ERA-40 reanalysis evaporation to the under representation of the irrigation areas in PCR-GLOBWB.

Contrary to the expectations, it appears that introducing an irrigation scheme in the hydrological model has negligible effect in the actual evaporation results for the resolution of $0.5^\circ \times 0.5^\circ$ used in this study. Only in some regions with very large irrigation areas, marginally higher evaporation was observed. However, we observed considerable differences in the evaporation results when the same irrigation scheme was introduced in a finer resolution model ($0.05^\circ \times 05^\circ$) for the Limpopo river basin. Therefore, it seems to be a resolution issue due to the small irrigation areas in Africa (with the exception of the Nile Delta) and the averaging in regions containing large non-irrigated areas.

4.3 Final remarks

This paper compares different evaporation products for Africa and presents an Actual Evaporation Multiproduct at a 0.5° resolution. This EM integrates satellite based products, evaporation results from land-surface models and from hydrological models forced with different precipitation and potential evaporation data sets. This product may serve as a reference data set (benchmark) and provide a range of variance in the expected actual evaporation values, which may be useful for water management applications in Africa. In general ERAI and MOD16 do not show good agreement with

HESSD

10, 8421–8465, 2013

Comparison of different evaporation estimates

P. Trambauer et al.

Title Page

Abstract

Introduction

Conclusions

References

Tables

Figures

◀

▶

◀

▶

Back

Close

Full Screen / Esc

Printer-friendly Version

Interactive Discussion



Comparison of different evaporation estimates

P. Trambauer et al.

Title Page

Abstract

Introduction

Conclusions

References

Tables

Figures

◀

▶

◀

▶

Back

Close

Full Screen / Esc

Printer-friendly Version

Interactive Discussion



other products in most part of Africa, while the rest of the products are more consistent. ERAI is generally quite close to the EM, and the higher values of evaporation in ERAI when compared with ERAL are partly explained by the soil moisture data assimilation in ERAI. It also appears that in some regions like in Southern Africa the agreement between the products is very good, which means that use of any of these products may be equally good. In other regions, such as in humid Sahel or the Mediterranean the choice of a particular product needs to be further studied as there is a larger difference between the products. A potential action to improve this comparison study and the EM is to validate the products in at least some African regions with ground data.

Acknowledgements. This study was carried out as part of the DEWFORA Project (“Improved Drought Early Warning and Forecasting to strengthen preparedness and adaptation to droughts in Africa”) which is funded by the Seventh Framework Programme for Research and Technological Development (FP7) of the European Union (Grant agreement no: 265454). Special acknowledgment goes to V. Thiemiig from JRC for providing pre-processed TRMM data for the African continent and to D. Miralles from the University of Bristol and VU Amsterdam for providing the global GLEAM dataset. The authors would like to thank G. Balsamo for the suggestions that helped to improve the manuscript.

References

- Alton, P., Fisher, R., Los, S., and Williams, M.: Simulations of global evapotranspiration using semiempirical and mechanistic schemes of plant hydrology, *Global Biogeochem. Cy.*, 23, GB4023, doi:10.1029/2009GB003540, 2009.
- Armstrong, R. L., Brodzik, M. J., Knowles, K., and Savoie, M.: Global monthly EASE-Grid snow water equivalent climatology, Boulder, CO: National Snow and Ice Data Center, Digital media, 2007.
- Balsamo, G., Beljaars, A., Scipal, K., Viterbo, P., van den Hurk, B., Hirschi, M., and Betts, A. K.: A Revised Hydrology for the ECMWF Model: Verification from Field Site to Terrestrial Water Storage and Impact in the Integrated Forecast System, *J. Hydrometeorol.*, 10, 623–643, 2009.

Comparison of different evaporation estimates

P. Trambauer et al.

Title Page

Abstract

Introduction

Conclusions

References

Tables

Figures

◀

▶

◀

▶

Back

Close

Full Screen / Esc

Printer-friendly Version

Interactive Discussion



- Balsamo, G., Boussetta, S., Lopez, P., and Ferranti, L.: Evaluation of ERA-Interim and ERA-Interim-GPCP-rescaled precipitation over the USA, ECMWF ERA Report Series 5, 1–25, available at: <http://www.ecmwf.int/publications/library/do/references/list/782009>, 2010.
- Balsamo, G., Pappenberger, F., Dutra, E., Viterbo, P., and van den Hurk, B.: A revised land hydrology in the ECMWF model: a step towards daily water flux prediction in a fully closed water cycle, *Hydrol. Process.*, 25, 1046–1054, 2011.
- Balsamo, G., Albergel, C., Beljaars, A., Boussetta, S., Brun, E., Cloke, H. L., Dee, D., Dutra, E., Pappenberger, F., Munoz Sabater, J., Stockdale, T., and Vitart, F.: ERA-Interim/Land: A global land-surface reanalysis based on ERA-Interim meteorological forcing, ECMWF ERA Report Series, Vol. 13, 1–25, 2012.
- Belo-Pereira, M., Dutra, E., and Viterbo, P.: Evaluation of global precipitation data sets over the Iberian Peninsula, *J. Geophys. Res.*, 116, D20101, doi:10.1029/2010JD015481, 2011.
- Cleugh, H. A., Leuning, R., Mu, Q., and Running, S. W.: Regional evaporation estimates from flux tower and MODIS satellite data, *Remote Sens. Environ.*, 106, 285–304, 2007.
- Dee, D. P., Uppala, S. M., Simmons, A. J., Berrisford, P., Poli, P., Kobayashi, S., Andrae, U., Balmaseda, M. A., Balsamo, G., Bauer, P., Bechtold, P., Beljaars, A. C. M., van de Berg, L., Bidlot, J., Bormann, N., Delsol, C., Dragani, R., Fuentes, M., Geer, A. J., Haimberger, L., Healy, S. B., Hersbach, H., Hólm, E. V., Isaksen, L., Kållberg, P., Köhler, M., Matricardi, M., McNally, A. P., Monge-Sanz, B. M., Morcrette, J. J., Park, B. K., Peubey, C., de Rosnay, P., Tavolato, C., Thépaut, J. N., and Vitart, F.: The ERA-Interim reanalysis: configuration and performance of the data assimilation system, *Q. J. Roy. Meteorol. Soc.*, 137, 553–597, 2011.
- Douville, H., Viterbo, P., Mahfouf, J. F., and Beljaars, A. C. M.: Evaluation of the Optimum interpolation and nudging techniques for soil moisture analysis using FIFE data, *Mon. Weather Rev.*, 128, 1733–1756, 2000.
- Droogers, P. and Allen, R.: Estimating Reference Evapotranspiration Under Inaccurate Data Conditions, *Irrig. Drain. Syst.*, 16, 33–45, 2002.
- FAO: Irrigation Potential in Africa: A Basin Approach, FAO, 1997.
- Global Aridity and PET Database: available at: <http://www.cgiar-csi.org> (last access: May 2012), 2010.
- Hargreaves, G. H. and Allen, R. G.: History and Evaluation of Hargreaves Evapotranspiration Equation, *J. Irrig. Drain. E.-ASCE*, 129, 53–63, 2003.
- Hijmans, R. J., Cameron, S. E., Parra, J. L., Jones, P. G., and Jarvis, A.: Very high resolution interpolated climate surfaces for global land areas, *Int. J. Climatol.*, 25, 1965–1978, 2005.

Comparison of different evaporation estimates

P. Trambauer et al.

Title Page

Abstract

Introduction

Conclusions

References

Tables

Figures

◀

▶

◀

▶

Back

Close

Full Screen / Esc

Printer-friendly Version

Interactive Discussion

- Huffman, G. J., Adler, R. F., Bolvin, D. T., and Gu, G.: Improving the global precipitation record: GPCP version 2.1, *Geophys. Res. Lett.*, 36, L17808, doi:10.1029/2009GL040000, 2009.
- Jacovides, C. P., Tymvios, F. S., Asimakopoulos, D. N., Theofilou, K. M., and Pashiardes, S.: Global photosynthetically active radiation and its relationship with global solar radiation in the Eastern Mediterranean basin, *Theor. Appl. Climatol.*, 74, 227–233, 2003.
- Jiménez, C., Prigent, C., Mueller, B., Seneviratne, S. I., McCabe, M. F., Wood, E. F., Rossow, W. B., Balsamo, G., Betts, A. K., Dirmeyer, P. A., Fisher, J. B., Jung, M., Kanamitsu, M., Reichle, R. H., Reichstein, M., Rodell, M., Sheffield, J., Tu, K., and Wang, K.: Global inter-comparison of 12 land surface heat flux estimates, *J. Geophys. Res.-Atmos.*, 116, D02102, doi:10.1029/2010jd014545, 2011.
- Keys, R.: Cubic convolution interpolation for digital image processing, *IEEE T. Acoust. Speech*, 29, 1153–1160, 1981.
- Kim, H. W., Hwang, K., Mu, Q., Lee, S. O., and Choi, M.: Validation of MODIS 16 global terrestrial evapotranspiration products in various climates and land cover types in Asia, *KSCE J. Civ. Eng.*, 16, 229–238, 2012.
- Kingston, D. G., Todd, M. C., Taylor, R. G., Thompson, J. R., and Arnell, N. W.: Uncertainty in the estimation of potential evapotranspiration under climate change, *Geophys. Res. Lett.*, 36, L20403, doi:10.1029/2009GL040267, 2009.
- Lau, K. M. and Wu, H. T.: Warm rain processes over tropical oceans and climate implications, *Geophys. Res. Lett.*, 30, 2290, doi:10.1029/2003GL018567, 2003.
- Liu, Y., Yamaguchi, Y., and Ke, C.: Reducing the discrepancy between ASTER and MODIS land surface temperature products, *Sensors*, 7, 3043–3057, 2007.
- McClain, M. E.: Balancing Water Resources Development and Environmental Sustainability in Africa: A Review of Recent Research Findings and Applications, *Ambio*, 1–17, doi:10.1007/s13280-012-0359-1, 2012.
- Miralles, D. G., De Jeu, R. A. M., Gash, J. H., Holmes, T. R. H., and Dolman, A. J.: Magnitude and variability of land evaporation and its components at the global scale, *Hydrol. Earth Syst. Sci.*, 15, 967–981, doi:10.5194/hess-15-967-2011, 2011a.
- Miralles, D. G., Holmes, T. R. H., De Jeu, R. A. M., Gash, J. H., Meesters, A. G. C. A., and Dolman, A. J.: Global land-surface evaporation estimated from satellite-based observations, *Hydrol. Earth Syst. Sci.*, 15, 453–469, doi:10.5194/hess-15-453-2011, 2011b.

HESSD

10, 8421–8465, 2013

Comparison of different evaporation estimates

P. Trambauer et al.

[Title Page](#)[Abstract](#)[Introduction](#)[Conclusions](#)[References](#)[Tables](#)[Figures](#)[⏪](#)[⏩](#)[◀](#)[▶](#)[Back](#)[Close](#)[Full Screen / Esc](#)[Printer-friendly Version](#)[Interactive Discussion](#)

- Mu, Q., Heinsch, F. A., Zhao, M., and Running, S. W.: Development of a global evapotranspiration algorithm based on MODIS and global meteorology data, *Remote Sens. Environ.*, 111, 519–536, 2007.
- Mu, Q., Zhao, M., and Running, S. W.: Improvements to a MODIS global terrestrial evapotranspiration algorithm, *Remote Sens. Environ.*, 115, 1781–1800, 2011.
- Mueller, B., Seneviratne, S. I., Jimenez, C., Corti, T., Hirschi, M., Balsamo, G., Ciais, P., Dirmeyer, P., Fisher, J. B., Guo, Z., Jung, M., Maignan, F., McCabe, M. F., Reichle, R., Reichstein, M., Rodell, M., Sheffield, J., Teuling, A. J., Wang, K., Wood, E. F., and Zhang, Y.: Evaluation of global observations-based evapotranspiration datasets and IPCC AR4 simulations, *Geophys. Res. Lett.*, 38, L06402, doi:10.1029/2010gl046230, 2011.
- Mueller, B., Hirschi, M., Jimenez, C., Ciais, P., Dirmeyer, P. A., Dolman, A. J., Fisher, J. B., Jung, M., Ludwig, F., Maignan, F., Miralles, D., McCabe, M. F., Reichstein, M., Sheffield, J., Wang, K. C., Wood, E. F., Zhang, Y., and Seneviratne, S. I.: Benchmark products for land evapotranspiration: LandFlux-EVAL multi-dataset synthesis, *Hydrol. Earth Syst. Sci. Discuss.*, 10, 769–805, doi:10.5194/hessd-10-769-2013, 2013.
- Overgaard, J., Rosbjerg, D., and Butts, M. B.: Land-surface modelling in hydrological perspective – a review, *Biogeosciences*, 3, 229–241, doi:10.5194/bg-3-229-2006, 2006.
- Owe, M., de Jeu, R., and Holmes, T.: Multisensor historical climatology of satellite-derived global land surface moisture, *J. Geophys. Res.-Earth*, 113, F01002, doi:10.1029/2007JF000769, 2008.
- Rossow, W. B. and Schiffer, R. A.: Advances in Understanding Clouds from ISCCP, *B. Am. Meteorol. Soc.*, 80, 2261–2287, 1999.
- Siebert, S., Döll, P., Feick, S., Hoogeveen, J., and Frenken, K.: Global Map of Irrigation Areas version 4.0.1, Rome, Italy, 2007.
- Sperna Weiland, F. C., Tisseuil, C., Dürr, H. H., Vrac, M., and van Beek, L. P. H.: Selecting the optimal method to calculate daily global reference potential evaporation from CFSR reanalysis data for application in a hydrological model study, *Hydrol. Earth Syst. Sci.*, 16, 983–1000, doi:10.5194/hess-16-983-2012, 2012.
- Sylla, M. B., Coppola, E., Mariotti, L., Giorgi, F., Ruti, P., Dell’Aquila, A., and Bi, X.: Multiyear simulation of the African climate using a regional climate model (RegCM3) with the high resolution ERA-interim reanalysis, *Clim. Dynam.*, 35, 231–247, 2010.



Comparison of different evaporation estimates

P. Trambauer et al.

Title Page

Abstract

Introduction

Conclusions

References

Tables

Figures

◀

▶

◀

▶

Back

Close

Full Screen / Esc

Printer-friendly Version

Interactive Discussion



- Szczypta, C., Calvet, J.-C., Albergel, C., Balsamo, G., Boussetta, S., Carrer, D., Lafont, S., and Meurey, C.: Verification of the new ECMWF ERA-Interim reanalysis over France, *Hydrol. Earth Syst. Sci.*, 15, 647–666, doi:10.5194/hess-15-647-2011, 2011.
- Teuling, A., Hirschi, M., Ohmura, A., Wild, M., Reichstein, M., Ciais, P., Buchmann, N., Ammann, C., Montagnani, L., and Richardson, A.: A regional perspective on trends in continental evaporation, *Geophys. Res. Lett.*, 36, L02404, doi:10.1029/2008GL036584, 2009.
- Thiemig, V., Rojas, R., Zambrano-Bigiarini, M., Levizzani, V., and De Roo, A.: Validation of Satellite-Based Precipitation Products Over Sparsely-Gauged African River Basins, *J. Hydrometeorol.*, 13, 1760–1783, doi:10.1175/JHM-D-12-032.1, 2012.
- UNEP: World atlas of desertification 2ED, UNEP (United Nations Environment Programme) London, 1997.
- MODIS Overview: available at: https://lpdaac.usgs.gov/products/modis_overview (last access: April 2012), 2012.
- van Beek, L. P. H. and Bierkens, M. F. P.: The Global Hydrological Model PCR-GLOBWB: Conceptualization, Parameterization and Verification, Utrecht University, Faculty of Earth Sciences, Department of Physical Geography, Utrecht, the Netherlands, 2009.
- van Beek, L. P. H., Wada, Y., and Bierkens, M. F. P.: Global monthly water stress: 1. Water balance and water availability, *Water Resour. Res.*, 47, W07517, doi:10.1029/2010WR009791, 2011.
- Van den Hurk, B., Viterbo, P., Beljaars, A. C. M., and Betts, A. K.: Offline validation of the ERA40 surface scheme, *ECMWF Tech. Memo.* 295, 1–42, 2000.
- van der Ent, R. J., Savenije, H. H. G., Schaefli, B., and Steele-Dunne, S. C.: Origin and fate of atmospheric moisture over continents, *Water Resour. Res.*, 46, W09525, doi:10.1029/2010WR009127, 2010.
- Vinukollu, R. K., Meynadier, R., Sheffield, J., and Wood, E. F.: Multi-model, multi-sensor estimates of global evapotranspiration: climatology, uncertainties and trends, *Hydrol. Process.*, 25, 3993–4010, doi:10.1002/hyp.8393, 2011.
- Wang, N.-Y., Liu, C., Ferraro, R., Wolff, D., Zipser, E., and Kummerow, C.: TRMM 2A12 Land Precipitation Product – Status and Future Plans, *J. Meteorol. Soc. Jpn. II*, 87A, 237–253, 2009.
- Weiß, M. and Menzel, L.: A global comparison of four potential evapotranspiration equations and their relevance to stream flow modelling in semi-arid environments, *Adv. Geosci.*, 18, 15–23, doi:10.5194/adgeo-18-15-2008, 2008.

Zhang, K., Kimball, J. S., Nemani, R. R., and Running, S. W.: A continuous satellite-derived global record of land surface evapotranspiration from 1983 to 2006, *Water Resour. Res.*, 46, W09522, doi:10.1029/2009WR008800, 2010.

5 Zomer, R. J., Trabucco, A., Bossio, D. A., van Straaten, O., and Verchot, L. V.: Climate Change Mitigation: A Spatial Analysis of Global Land Suitability for Clean Development Mechanism Afforestation and Reforestation, *Agr. Ecosyst. Environ.*, 126, 67–80, 2008.

HESSD

10, 8421–8465, 2013

Comparison of different evaporation estimates

P. Trambauer et al.

Title Page

Abstract

Introduction

Conclusions

References

Tables

Figures

⏪

⏩

◀

▶

Back

Close

Full Screen / Esc

Printer-friendly Version

Interactive Discussion



HESSD

10, 8421–8465, 2013

Comparison of different evaporation estimates

P. Trambauer et al.

Table 1. Summary of African Evaporation Products used in this study.

Evaporation Product	Provider	Input precipitation data	Potential Evaporation – Method	Spatial resolution	Temporal coverage
[1] PCR-GLOBWB	This study*	ERA1 + GPCP	Hargreaves	0.5°	1 Jan 1979–31 Dec 2010
[2] PCR_PM	This study*	ERA1 + GPCP	Penman Monteith	0.5°	1 Jan 1979–31 Dec 2010
[3] PCR_TRMM	This study*	TRMM 3B42 v6	Hargreaves	0.5°	Since 1 Jan 1998
[4] PCR_Irrig	This study*	ERA1 + GPCP	Hargreaves	0.5°	1 Jan 1979–31 Dec 2010
[5] ERA1	ECMWF	ERA1	No PE input	~ 0.7°	1 Jan 1979–near real-time
[6] ERA1	ECMWF	ERA1 + GPCP	No PE input	~ 0.7°	1 Jan 1979–31 Dec 2010
[7] MOD16	University of Montana	NASA's GMAO	Penman Monteith	1 km	Since 1 Jan 2000
[8] GLEAM	VU Amsterdam	PERSIANN	No PE input	0.25°	Since 1 Jan 2000

* The evaporation product resulted from the PCR-GLOBWB hydrological model (van Beek and Bierkens, 2009) forced with different (varying) input data and conditions.

[Title Page](#)[Abstract](#)[Introduction](#)[Conclusions](#)[References](#)[Tables](#)[Figures](#)[⏪](#)[⏩](#)[◀](#)[▶](#)[Back](#)[Close](#)[Full Screen / Esc](#)[Printer-friendly Version](#)[Interactive Discussion](#)

HESD

10, 8421–8465, 2013

Comparison of different evaporation estimates

P. Trambauer et al.

[Title Page](#)[Abstract](#)[Introduction](#)[Conclusions](#)[References](#)[Tables](#)[Figures](#)[I ◀](#)[▶ I](#)[◀](#)[▶](#)[Back](#)[Close](#)[Full Screen / Esc](#)[Printer-friendly Version](#)[Interactive Discussion](#)

Table 2. Generalized climate classification scheme for Global-Aridity values (UNEP, 1997).

Aridity Index Value	Climate Class
< 0.03	Hyper Arid
0.03–0.2	Arid
0.2–0.5	Semi-Arid
0.5–0.65	Dry sub-humid
> 0.65	Humid

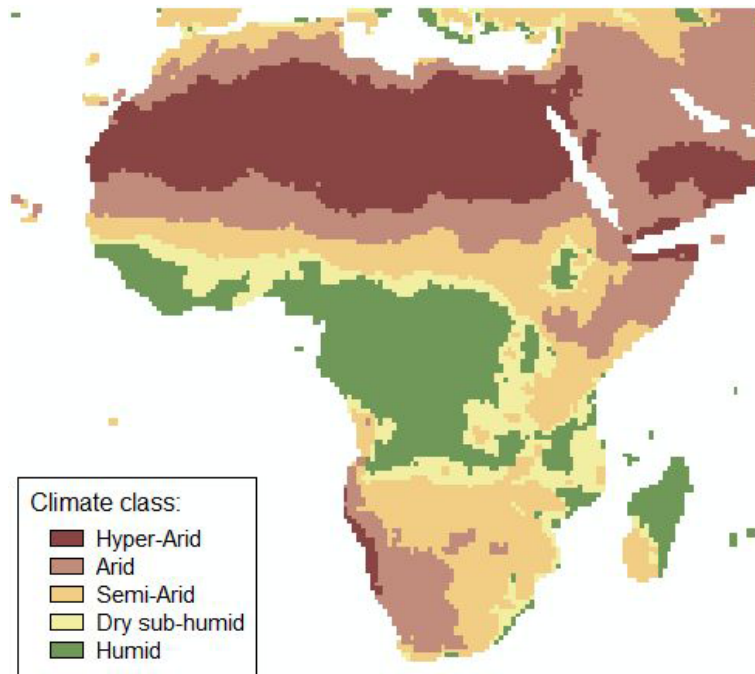


Fig. 1. Derived Climate classes for the African continent with a resolution of 0.5 degrees.

Comparison of different evaporation estimates

P. Trambauer et al.

Title Page

Abstract

Introduction

Conclusions

References

Tables

Figures

◀

▶

◀

▶

Back

Close

Full Screen / Esc

Printer-friendly Version

Interactive Discussion



Comparison of different evaporation estimates

P. Trambauer et al.

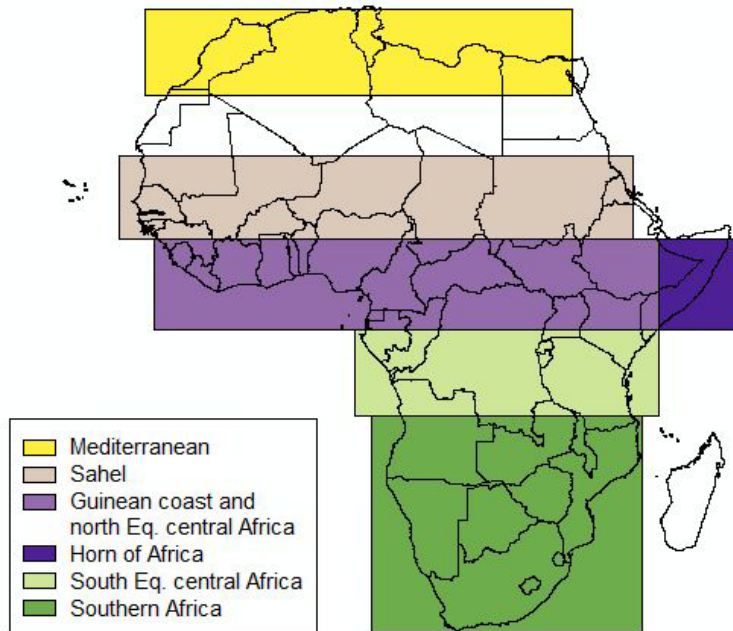


Fig. 2. Location-regions in Africa.

[Title Page](#)[Abstract](#)[Introduction](#)[Conclusions](#)[References](#)[Tables](#)[Figures](#)[◀](#)[▶](#)[◀](#)[▶](#)[Back](#)[Close](#)[Full Screen / Esc](#)[Printer-friendly Version](#)[Interactive Discussion](#)

Comparison of different evaporation estimates

P. Trambauer et al.

Title Page

Abstract

Introduction

Conclusions

References

Tables

Figures

◀

▶

◀

▶

Back

Close

Full Screen / Esc

Printer-friendly Version

Interactive Discussion

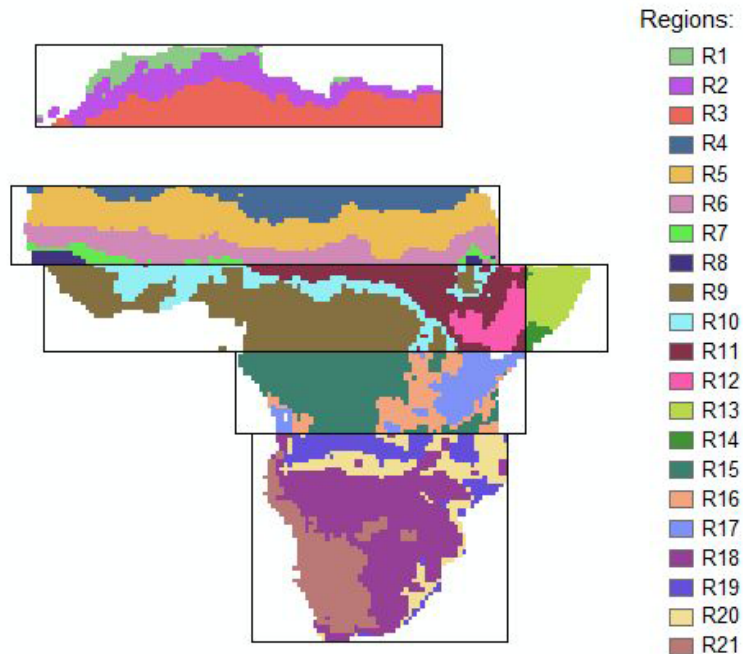


Fig. 3. Derived “Regions”.

Comparison of different evaporation estimates

P. Trambauer et al.

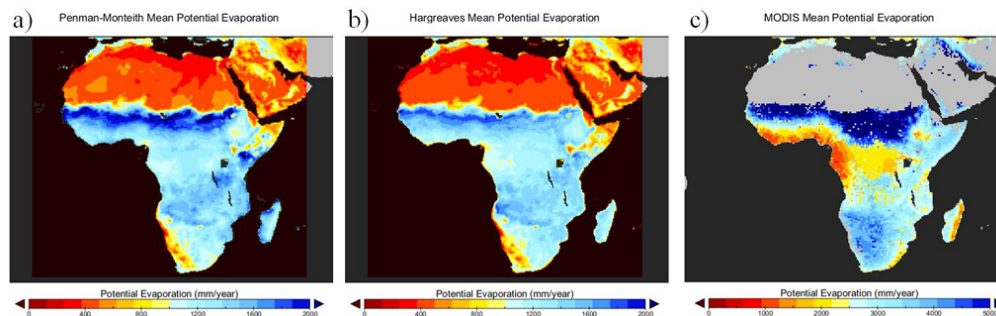


Fig. 4. Comparison of mean annual crop-specific potential evaporation computations for Africa with different methods: **(a)** Penman-Monteith, **(b)** Hargreaves and **(c)** MOD16 product (note that the grey area corresponds to missing data and that values are presented at another scale to improve visualization).

[Title Page](#)[Abstract](#)[Introduction](#)[Conclusions](#)[References](#)[Tables](#)[Figures](#)[⏪](#)[⏩](#)[◀](#)[▶](#)[Back](#)[Close](#)[Full Screen / Esc](#)[Printer-friendly Version](#)[Interactive Discussion](#)

Comparison of different evaporation estimates

P. Trambauer et al.

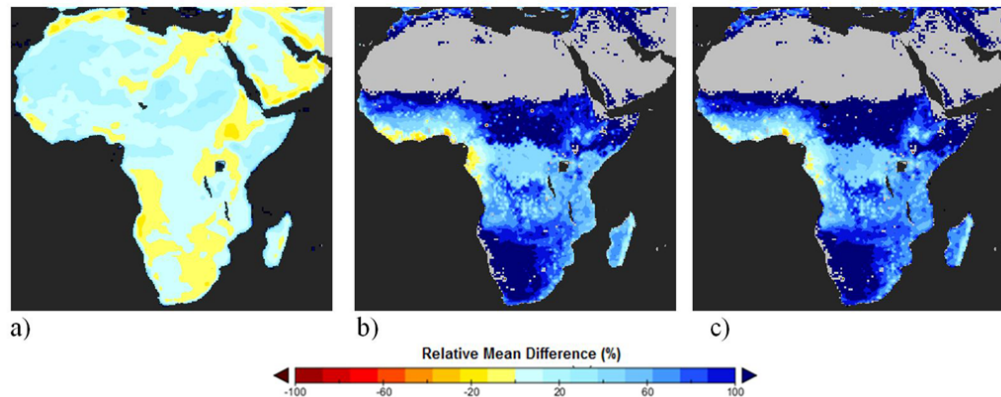


Fig. 5. Relative mean difference (RMD) between: **(a)** Penman-Monteith potential evaporation (PE) and Hargreaves PE, **(b)** MOD16 PE and Penman-Monteith PE, and **(c)** MOD16 PE and Hargreaves PE.

[Title Page](#)[Abstract](#)[Introduction](#)[Conclusions](#)[References](#)[Tables](#)[Figures](#)[◀](#)[▶](#)[◀](#)[▶](#)[Back](#)[Close](#)[Full Screen / Esc](#)[Printer-friendly Version](#)[Interactive Discussion](#)

**Comparison of
different evaporation
estimates**

P. Trambauer et al.

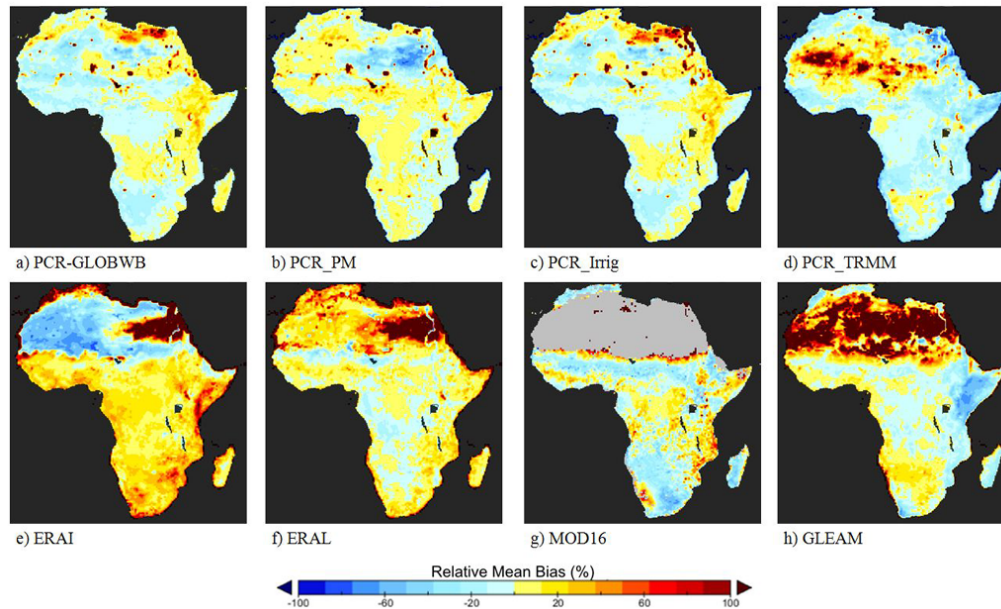


Fig. 6. Relative Mean Bias (RMB) between each product and the evaporation multiproduct (EM).

[Title Page](#)[Abstract](#)[Introduction](#)[Conclusions](#)[References](#)[Tables](#)[Figures](#)[◀](#)[▶](#)[◀](#)[▶](#)[Back](#)[Close](#)[Full Screen / Esc](#)[Printer-friendly Version](#)[Interactive Discussion](#)

Comparison of different evaporation estimates

P. Trambauer et al.

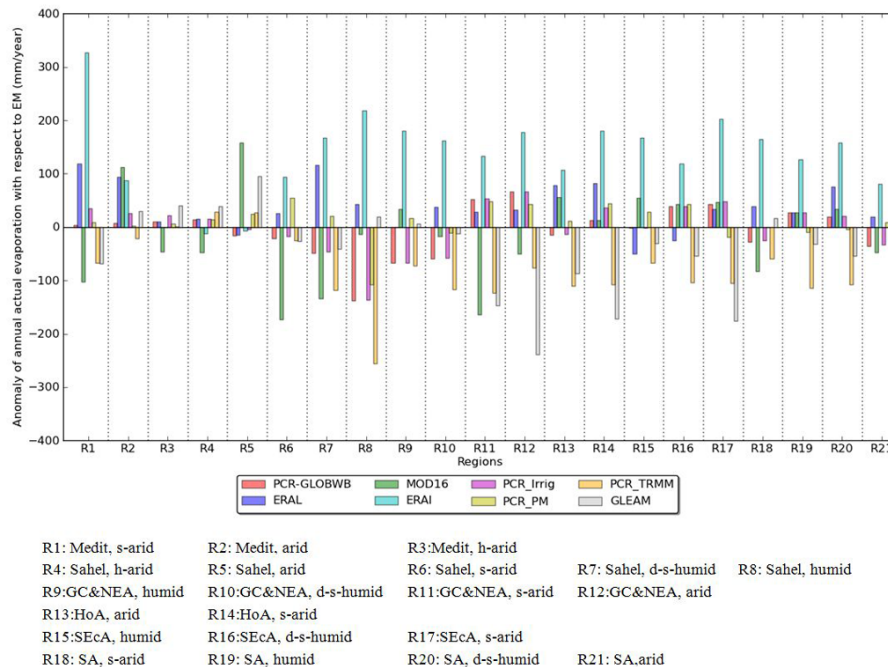


Fig. 7. Annual anomaly of evaporation for each product with respect to the evaporation multi-product (EM) for each region.

Title Page

Abstract

Introduction

Conclusions

References

Tables

Figures

◀

▶

◀

▶

Back

Close

Full Screen / Esc

Printer-friendly Version

Interactive Discussion



Comparison of different evaporation estimates

P. Trambauer et al.

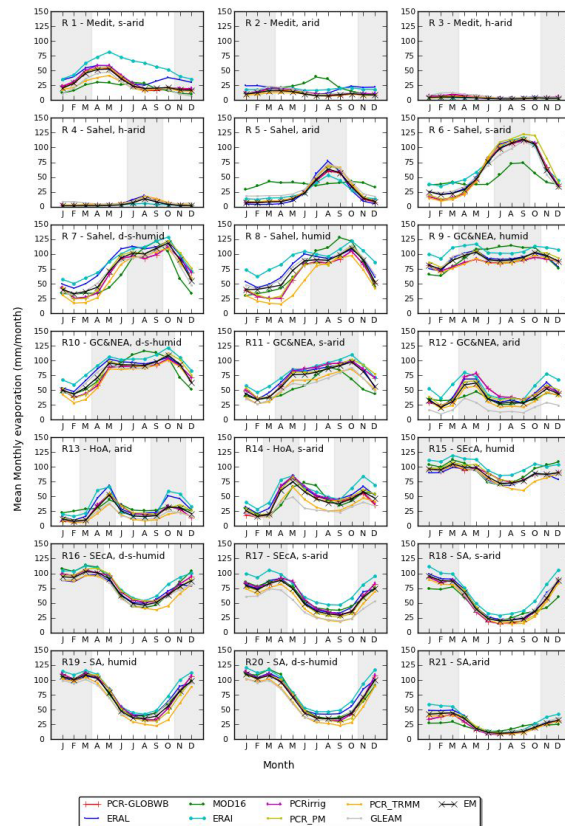


Fig. 8. Interannual variation of mean monthly actual evaporation for each region. In grey, the wet periods, and in white the dry periods according to Sylla et al. (2010) and Jacovides et al. (2003). MOD16 product is not presented in hyper-arid areas (R3 and R4) plots due to unavailability of data for these areas.

[Title Page](#)
[Abstract](#)
[Introduction](#)
[Conclusions](#)
[References](#)
[Tables](#)
[Figures](#)
[Back](#)
[Close](#)
[Full Screen / Esc](#)
[Printer-friendly Version](#)
[Interactive Discussion](#)

HESSD

10, 8421–8465, 2013

Comparison of different evaporation estimates

P. Trambauer et al.

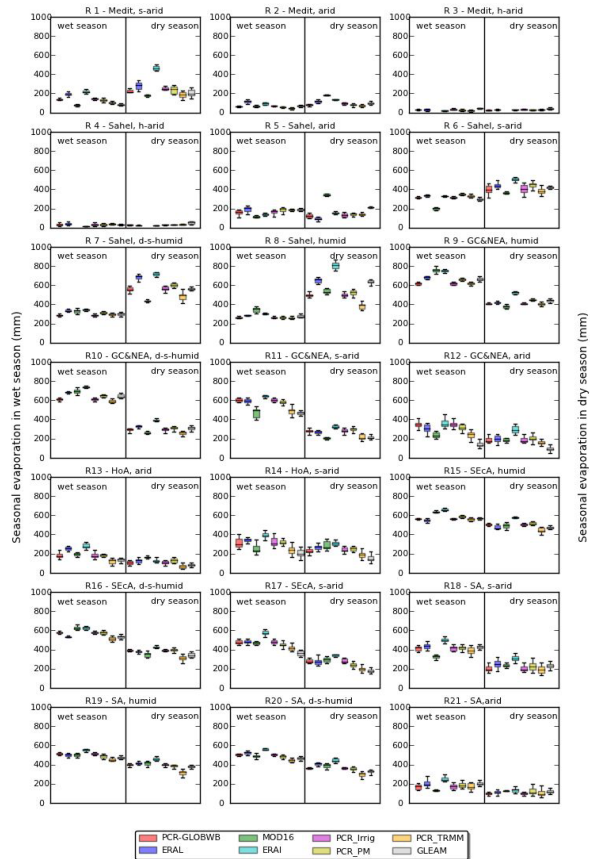


Fig. 9. Box-plot diagrams of seasonal evaporation for each region.

Title Page

Abstract

Introduction

Conclusions

References

Tables

Figures

⏪

⏩

◀

▶

Back

Close

Full Screen / Esc

Printer-friendly Version

Interactive Discussion



Comparison of different evaporation estimates

P. Trambauer et al.

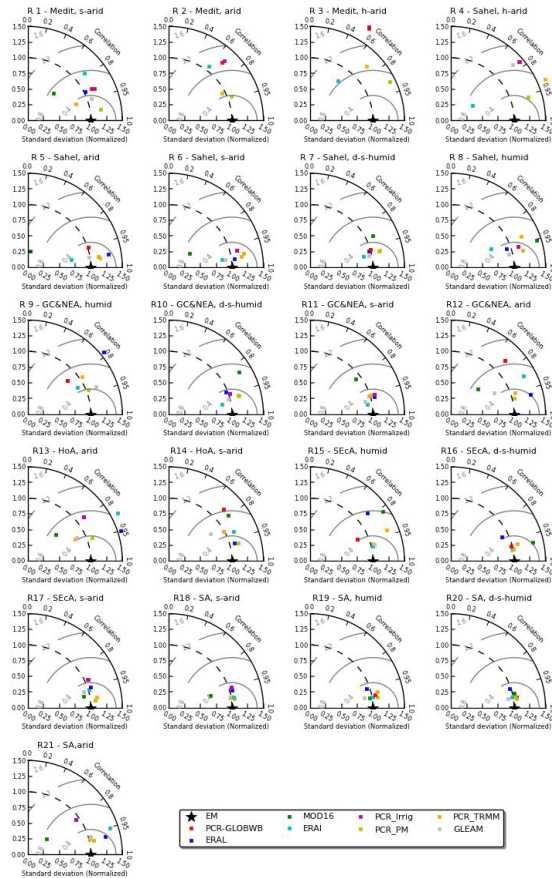


Fig. 10. Taylor diagrams summarizing the statistics between the monthly time series of the different products assuming the EM is the “reference”.

[Title Page](#)

[Abstract](#)

[Introduction](#)

[Conclusions](#)

[References](#)

[Tables](#)

[Figures](#)

[⏪](#)

[⏩](#)

[⏴](#)

[⏵](#)

[Back](#)

[Close](#)

[Full Screen / Esc](#)

[Printer-friendly Version](#)

[Interactive Discussion](#)



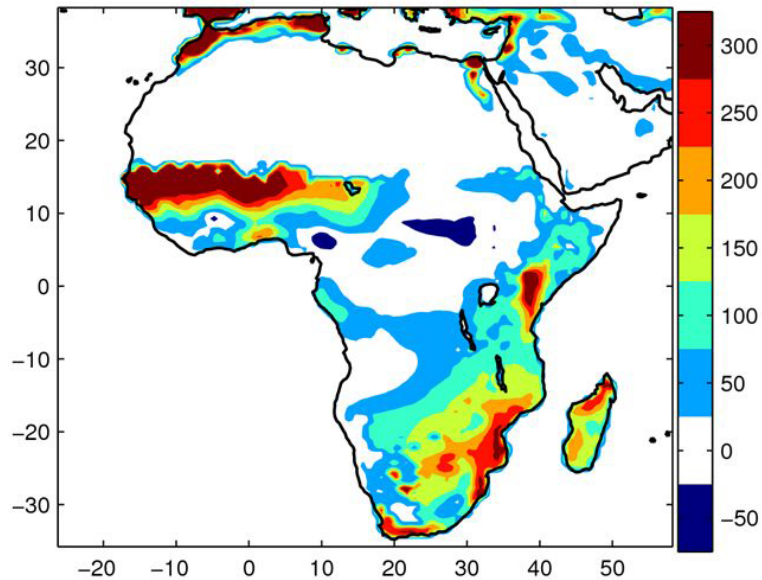


Fig. 11. Mean annual soil moisture increments (in mm yr^{-1}) in ERA-I.

Comparison of different evaporation estimates

P. Trambauer et al.

[Title Page](#)

[Abstract](#) [Introduction](#)

[Conclusions](#) [References](#)

[Tables](#) [Figures](#)

[◀](#) [▶](#)

[◀](#) [▶](#)

[Back](#) [Close](#)

[Full Screen / Esc](#)

[Printer-friendly Version](#)

[Interactive Discussion](#)

